Experimental measurements of laminar flame speeds for highly N2-diluted ethanol flames under microgravity conditions

Chaimae Bariki, Fabien Halter, Raik Hesse, Christian Chauveau, Heinz Pitsch, Joachim Beeckmann

Experimental measurements of laminar flame speeds for highly N_2-diluted ethanol flames under microgravity conditions

Chaimae Bariki[a,*], Fabien Halter[b,c], Raik Hesse[a], Christian Chauveau[b], Heinz Pitsch[a], Joachim Beeckmann[a]

[a] *Institute for Combustion Technology, RWTH Aachen University, 52056 Aachen, Germany*
[b] *CNRS ICARE, Avenue de la Recherche Scientifique, 45071 Orléans Cedex 2, France*
[c] *University of Orléans, Orléans Cedex 2, France*

Abstract

Nitrogen has been used as an alternative for CO_2 in the fire suppression industry. The high nitrogen concentrations added to a reactive mixture slows down its flame propagation in case of a fire outbreak. To describe quantitatively the flame spread as a function of nitrogen dilution, it is mandatory to evaluate the mixture's laminar flame speed. Performing experiments under earth gravity using the RWTH high-pressure, high-temperature spherical combustion chamber showed that the laminar flame speed extraction is impossible for such highly dilute conditions due to severe flame-front distortions. To overcome the influence of buoyancy, experiments were carried out under microgravity conditions in a parabolic flight campaign onboard the Airbus A310 Zero-G. The setup consists of a pressure-release-type dual chamber adequate for aircraft-related safety requirements, and a conventional shadowgraphy system to visualize the flame morphology under quasi-isobaric pressure. Only a limited number of liquid energy carriers are allowed onboard, and ethanol was chosen because of its short molecular structure and low boiling point compared to longer chain liquid alkanes such as n-heptane. Results showed a flame speed reduction induced by radiation in the order of 10% to 45% for near-stoichiometric to very rich conditions, respectively. To correct laminar flame speeds for radiation effects, an empirical correlation presented by Yu et al. (Combust. Flame 161 (2014) 2815-2824) is applied. Excellent agreement between radiation-corrected experimental data and simulations using the chemical mechanism of Cai et al. (Combust. Flame 37 (2019) 639-647) is found. This indicates that high dilution levels with nitrogen can be captured well by kinetic schemes derived for fast-burning flames. The unique experimental data obtained here, which were extremely difficult to measure and post-processed very carefully, can be used as a reference to validate/improve existing and newly developed kinetic mechanisms.

Keywords: Buoyancy; Microgravity; Laminar Flame Speed; Spherical Flame; Radiation

1. Introduction

Chemically inert diluents, such as nitrogen, have proven to be an important class of fire extinguishing agents in confined environments such as spacecraft [1–3]. Nitrogen is safe for use in occupied spaces and poses no threat to the environment. Several studies focused on assessing flame extinction limits caused by N_2 diluent [4] and its effects on ignition processes [3]. Flame propagation is also an aspect investigated by several groups since it also occurs in the fire suppression process [1, 2, 5]. Highly N_2-diluted flames are slow-burning near the flammability limits. They are affected both by radiation heat losses and buoyancy. As a result, these flames are heavily distorted due to the gravitational force and are prone to experimental errors. It is worth stressing that the available experimental data measured for slow propagating flames are sparse in the literature. In addition, modeling real fuels is difficult because these are mixtures of hundreds of components, making it challenging to unravel their combustion chemistry. For this reason, fuel surrogates containing simpler mixtures of well-selected components are used to model the combustion behavior. This study is essential for a fundamental understanding of (1) how fast flames are when approaching the flammability limit and (2) how radiation heat losses affect flame propagation. Experiments and simulations are used to highlight the complexity of extracting accurate flame speeds of such slowly propagating flames, even for well-known fuels.

The laminar flame speed is a fundamental physicochemical property of a combustible mixture because it notably influences the mixture's burning rate. Measuring the laminar flame speed is essential for validating kinetic mechanisms [6] and serves as an input parameter in turbulent combustion models [7]. An accurate measurement of this property for slowly propagating flames is difficult because the effects of gravity and radiation cannot be neglected anymore. Owing to these difficulties, measuring the laminar flame speeds of highly diluted premixed mixtures remains a formidable challenge.

The closed vessel method with spherically propagating flames has been widely used to measure the laminar flame speed due to its large pressure-range applicability and well-defined stretch rate. For slowly burning flames, the gravitational force can lead to a strong deformation of the initially spherical shape, making the extraction of this parameter extremely difficult. The methods found in the literature to assess buoyant flames differ quite significantly between studies. For example, Pfahl et al. [8] suggested a method evaluating only the horizontal radii temporal evolution of optically investigated flames in a spherical vessel. Accordingly, Sun et al. [9] proposed two parameters, a buoyant flow rate, and a buoyant critical flame radius, to investigate gravity effects quantitatively from the flame front's projection area determined using a Schlieren technique. Recently, Berger et al. [10] analyzed the effect of buoyancy through direct numerical simulations (DNS) of spherically expanding laminar premixed flames whose motion is affected by buoyancy. They proposed a new technique to extract the laminar flame speed. However, it cannot be directly determined from experimental images recorded during the flame propagation. The robustness and validity of existing post-processing techniques for slowly burning flames are still unclear and the only way to suppress buoyancy effects is to conduct experiments under microgravity conditions, for example in a drop tower facility or on a parabolic flight.

Radiative heat losses inherently affect laminar flame speeds measured in a spherical chamber and can no longer be neglected for slowly propagating flames, as it was recently demonstrated by Hegetschweiler et al. [11] and Hesse et al. [12]. As propagation time increases, radiation plays an increasingly important role due to the cooling of burned gases. Several correction schemes relying on empirical corrections or thermodynamics were proposed for spherically expanding flames measured under quasi-isobaric conditions. These models were almost exclusively applied to standard hydrocarbons or hydrogen, which have significantly faster flame speeds than highly N_2-diluted flames. Yet, the nitrogen chemistry has not been taken into account in the radiation correction models. For instance, Santner et al. [13] proposed a correction based on a thermodynamic calculation to correct for radiation. This approach estimates the thermal and flow effects caused by radiation separately. Yu et al. [14] proposed an empirical correlation approach, which has been validated for flame speeds of 10 cm/s and faster. However, there is no proof that it can be applied to mixtures resulting in flame speeds below 10 cm/s, such as conditions encountered during the combustion of highly N_2-diluted mixtures or fuels such as ammonia and refrigerants.

Given these considerations, the main goal of the present paper is to investigate the combined effects of stretch and radiation on N_2-diluted premixed spherically expanding flames. First, measurements were conducted under terrestrial gravity to elucidate the flame distortion issue due to the gravitational force and the difficulty in extracting the laminar flame speed based on the existing models. Second, experiments were carried out in a pressure-release-type dual chamber, adequate for aircraft-related safety requirements, during parabolic flights onboard the Airbus A310 Zero-G to suppress the buoyancy effect under microgravity conditions. Since only a few selected liquid fuels are allowed onboard the aircraft, ethanol was chosen for this work.

2. Experimental framework

2.1. Experimental setups

Experiments were conducted under microgravity

conditions to suppress the effect of buoyancy for slowly propagating flames in a pressure-release-type dual chamber, which is adequate for aircraft-related safety requirements [15, 16]. These conditions were obtained using the parabolic flights of the Airbus A310 ZERO-G, during which a 10^{-2} g gravity level is achieved. A schematic of the experimental facility is given in Fig. 1. It consists of a 1 L spherical chamber inserted in an 11 L high-pressure chamber. The spherical combustion chamber is equipped with eight symmetrically distributed evacuation valves to release pressure during flame propagation once 0.025 MPa increase is reached. Note that in all cases, pressure release occurs largely after the flame exceeded the window limit. The pressure variation is very low although the flame has traveled half the chamber radius. The inner chamber is filled with the flammable mixture, while the high-pressure chamber is filled at the same time with nitrogen.

Liquid fuel injection is performed using a multi-injection system with a switching valve which delivers an accurate volume of ethanol to obtain the targeted equivalence ratio. The fresh gases are heated by an electric heating cable that encircles the chamber. Additionally, a pre-heater is used to pre-vaporize the air-fuel mixture before it arrives in the combustion chamber. A K-type thermocouple of 13 μm diameter and a pressure sensor monitor the temperature and the pressure during the filling process.

Both chambers are equipped with aligned transparent windows to allow optical access. A conventional shadowgraphy system is used to visualize the flame morphology. An Energetiq LDLS (Laser-Driven-Light-Source) is used as light source, and a high-speed camera (Phantom v1210) continuously records the flame propagation at 1000 fps, with a field of view of 768 $\times$ 768 pixels^2. The resulting magnification ratio is 16.4 px/mm.

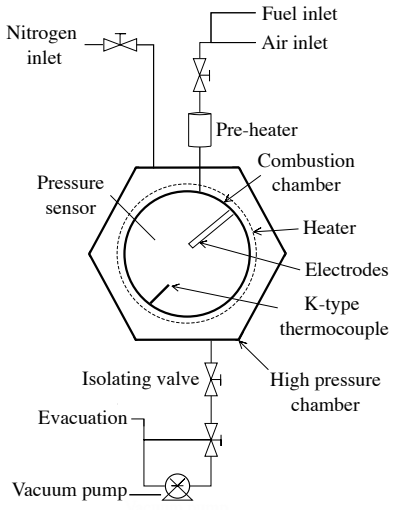

Fig. 1: Schematic of the parabolic flight setup.

The combustible mixtures were ignited at the chamber's center using a pair of tungsten electrodes of 0.3 mm diameter, arranged face to face. The electrode distance was set to 1.5 mm. The spark was generated using a newly developed two-step high-voltage system: the first output stage feeds an ignition coil, which is responsible for ionizing the mixture between the electrodes and generating the primary ignition spark. If the mixture is conductive, the current can flow through the gap between the electrodes allowing the second stage of the ignition system to feed more energy into the spark. A variable voltage of 500 to 1800 V DC, fed by the power capacitors, can be generated. More details are given in the Supplementary Material for completeness. The applied voltage and its corresponding delivered energy are reported in Table 1.

Table 1: Applied voltage and delivered energy output in air by the high-voltage ignition system using a 1.5 mm gap at the electrode tips at 1 atm.

Voltage [kV]	0.50	0.80	1.00	1.30	1.50	1.80
Energy [J]	0.24	0.92	1.62	3.05	4.25	6.43

Experiments under terrestrial gravity conditions were conducted in the RWTH high-pressure, high-temperature spherical chamber [17–19]. The schematic of the setup and the respective characteristic parameters are given in Fig. S1 and Table S1 of the Supplementary Material, and only a brief description is given here. Flame propagation is imaged with a Schlieren technique. A pulsed high-power LED emitting green light is used with a high-speed CMOS camera (LaVision HighSpeedStar 6). The acquisition rate was set to 5 kHz with a field of view of 448 $\times$ 448 pixels^2 resulting in a magnification ratio of 11.41 px/mm. All fuel/air mixtures were prepared in a separate premixing vessel using the partial pressure method. Two temperature-compensated pressure transducers were used during the mixture preparation with different ranges of 3 and 10 bar to accurately perform the filling process. The combustible mixtures were ignited at the chamber's center using a pair of tungsten electrodes of 0.3 mm diameter, arranged face to face, with an electrode distance of 1.5 mm. The spark was generated using a similar two-step high-voltage system as the one used for parabolic flight experiments.

2.2. Selected conditions

For aircraft-related safety reasons, gaseous fuels, such as ammonia and refrigerants, are prohibited, and only a few selected liquid fuels are allowed onboard the aircraft. Radiation is caused mainly by the combustion products H_2O and CO_2 and by soot. Here, a fuel with high sooting propensity was not chosen because the windows would become dirty after only a few measurements under microgravity conditions. This is a critical point to be considered, given the short time between parabolas. Therefore,

Table 2: Experimental investigated conditions under microgravity and earth gravity conditions of ethanol mixtures.

	Fuel	Oxidizer (% in vol.)	T_0 [K]	P_0 [bar]	Equivalence ratio ϕ [-]
0 g	Ethanol	12% O_2 / 88% N_2	373	1	1.23
	Ethanol	12% O_2 / 88% N_2	373	3	1.06, 1.23, 1.37, 1.52, 1.66
	Ethanol	12% O_2 / 88% N_2	373	5	0.81, 1.06, 1.23, 1.4, 1.58
	Ethanol	12% O_2 / 88% N_2	373	7	1.23
1 g	Ethanol	12% O_2 / 88% N_2	373	3	1.4
	Ethanol	12% O_2 / 88% N_2	373	10	1.4

ethanol was selected to avoid this problem and still be able to evaluate radiation effects. Moreover, previous campaigns widely investigated this fuel in the parabolic flight setup at conditions facilitating significantly faster flame speeds. One way to obtain highly-buoyant flames is to decrease the content of oxygen. A preliminary parametric study was conducted to define the content of oxygen to be used, and it was found that a synthetic mixture of 12% O_2 and 88% N_2 in volume is sufficient to obtain medium- to highly-buoyant flames under normal-gravity conditions. The severity of the buoyancy impact was varied by approaching lean and rich flammability limits. Note that it is unnecessary to modify the O_2 content to obtain buoyant flames near the fuel-rich flammability limit, which corresponds to 9.8% for ethanol [20]. Decreasing the O_2 content reduces not only the flame temperature but also the flame speed and the propensity for cellular structure formation, thus, enabling the analysis of radiation and buoyancy effects independently. Note that the effect of buoyancy is governed by the Richardson number, which is defined as $\mathrm{Ri} = (\rho_\mathrm{u} - \rho_\mathrm{b})/\rho_\mathrm{u} \cdot \mathrm{g} R_\mathrm{f}/\dot{R}_\mathrm{f}^2$. Here, ρ_u and ρ_b represent the density in the unburned and burned gas, g is the gravitational acceleration, R_f is the flame radius, and $\dot{R}_\mathrm{f}$ refers to the propagation speed.

An initial temperature was fixed at 373 K for all conditions. It is important to highlight that igniting the selected mixtures would not be possible without the newly developed high-voltage ignition system and measurements under these conditions were extremely challenging. Table 2 summarizes the experimental conditions investigated. The repeatability of the results was ensured by conducting two to three experiments for each condition.

3. Simulation framework

Flame characteristics were calculated for a 1D unstretched laminar flame configuration, using the open-source FlameMaster code [21]. The ITV chemical mechanism developed by Cai et al. [22], which was validated extensively for a large number of fuels including ethanol, was chosen to compare experimental and predicted results.

In order to ensure that the mechanism by Cai et al. [22] is valid for the investigated conditions, an indicative sensitivity analysis has been performed for different ethanol mixtures to identify the key reactions influencing laminar flame speeds. Sensitivity coefficients $S^{\alpha}_{S_\mathrm{L}}$ on elementary reaction rate constants for an initial pressure of 3 bar were calculated as

$$S^{\alpha}_{S_\mathrm{L}} = \frac{k_\alpha}{S_\mathrm{L}} \frac{\mathrm{d}S_\mathrm{L}}{\mathrm{d}k_\alpha}. \quad (1)$$

Here, k_α is the rate constant of reaction α of the chemical mechanism. Three dilution rates of 21/79, 16/84, and 12/88 O_2/N_2 were considered. The sensitivity coefficients are shown in Fig. 2 for stoichiometric mixture condition. As expected, small-species reactions such as H + O_2 ↔ O + OH, CO + OH ↔ CO_2 + H and HCO (+ M) ↔ H + CO (+ M) are important reactions that enhance flame reactivity, while the reactions CH_3 + H (+ M) ↔ CH_4 (+ M) and H + O_2 (+ M) ↔ HO_2 (+ M) reduce flame speed predictions for all mixtures. The fuel-specific reactions with considerable sensitivities are the H-abstraction reactions by hydrogen radical, which have a mild negative sensitivity, and those by hydroxyl radical, which have a small positive sensitivity. Similar behaviors are observed for the three dilution rates in Fig. 2. One can deduce that the reaction pathways are not strongly influenced when decreasing the content of oxygen.

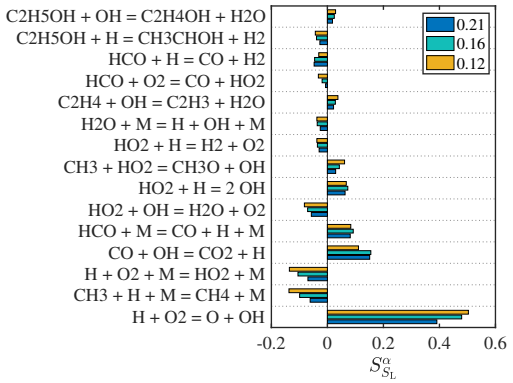

Fig. 2: Laminar flame speed sensitivities on reaction rate coefficients of ethanol mixtures with various dilution rates using the Cai et al. model [22] ($\phi = 1.0$, $P_0 = 3$ bar, $T_0 = 373$ K).

4. Results and discussion

4.1. Terrestrial gravity measurements

Experiments were conducted under terrestrial gravity conditions, and the temporal evolution of the typical Schlieren images recorded are shown in Fig. 3. During the first phase of the flame at an initial pressure of 3 bar (cf. Fig. 3 (first row)), it propagates spherically. As the flame continues to grow, the gravitational force leads to a strong deformation of the initially spherical shape. Due to the substantial density difference between the burned and unburned gas, the flame develops an upward motion, leading to a flame deformation and attaining a mushroom-like shape. After reaching the top of the chamber, the flame spreads laterally and downward to consume the remaining mixture in the combustion chamber.

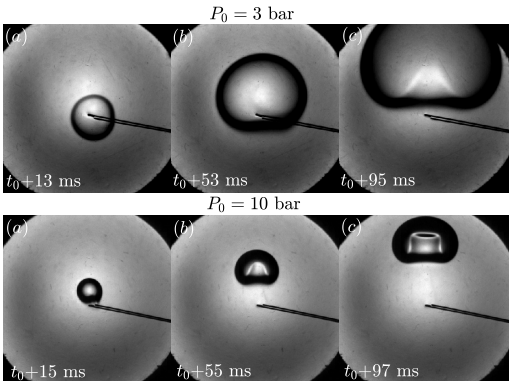

Fig. 3: Sequence of typical Schlieren images of highly-buoyant ethanol flames under terrestrial gravity obtained using the RWTH setup ($\phi = 1.4$, $T_0 = 373$ K, $P_0 = 3$ and 10 bar, oxidizer: 12% O_2 - 88% N_2 in vol.).

By further increasing the initial pressure to 10 bar (cf. Fig. 3 (second row)), the flame motion is significantly affected by buoyancy. It can be seen that the upward flame motion induces entrainment of unburned gas beneath the flame, resulting in a complex flow. Consequently, different points of the flame front propagate with different absolute speeds, making the extraction of laminar flame speed extremely difficult. Similar behavior was recently reported by Berger et al. [10] where DNS of spherically expanding premixed flames were performed for flames featuring very low flame speeds. Existing post-processing techniques, such as the horizontal radius or the equivalent radius based on the flame's cross-section, are not feasible for these highly buoyant flames. Extracting the correct flame-front contour is extremely challenging, especially beneath the flame. An advanced optical technique, such as particle image velocimetry (PIV), would need to be used to overcome this problem. This is not discussed further because it is out of the scope of the present paper. To extract the laminar flame speed accurately for these highly-buoyant flames based on the recorded images, experiments under microgravity conditions are necessary to suppress the formation of these non-spherical shapes.

4.2. Microgravity measurements

A series of parabolic flights onboard the Airbus A310 Zero-G was conducted under microgravity conditions to suppress the effect of buoyancy for slowly propagating ethanol/O_2/N_2 flames. An example is given as in Fig. 4 for a fuel-rich ethanol flame obtained at two initial pressures. For both conditions (i.e., $P_0 = 3$ and 5 bar), the flame expands in an almost perfectly spherical manner until it reaches the limit of the window. Only images corresponding to a flame front radius greater than 9 mm were used to overcome ignition effects. It is worth stressing that the usable data range is larger than for terrestrial gravity experiments where flames quickly reach the upper windows' limit.

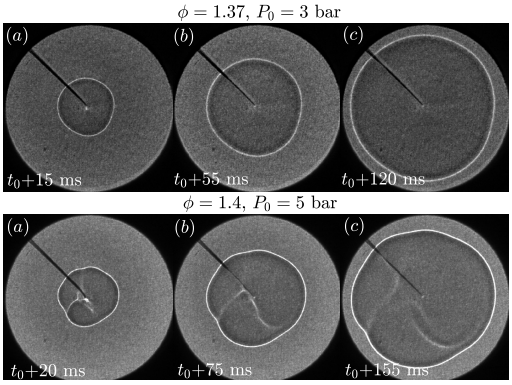

Fig. 4: Sequence of typical shadowgraph images of ethanol flames under microgravity conditions during parabolic flights ($T_0 = 373$ K, oxidizer: 12% O_2 - 88% N_2 in vol.). (a), (b) and (c) correspond to a flame radius of 0.8 cm, 1.4 cm, and 1.8 cm, respectively.

The temporal evolution of the flame radius $R_\mathrm{f}(t)$ is extracted from the shadowgraph images. The flame front temperature gradient is highlighted as a bright/dark interface. A post-processing script was used to deduce the instantaneous flame front radius from the projected spherical flame surface. The propagation speed with respect to the burned mixture is determined as $S_\mathrm{L,b} = \mathrm{d}R_\mathrm{f}/\mathrm{d}t$. The normalized rate-of-change in flame surface area, A_f, constitutes the total stretch rate K. In case of a spherical flame, the latter is written as $K = 2S_\mathrm{L,b}/R_\mathrm{f}$.

4.2.1. Flame propagation speed

Figure 5 depicts the evolution of the measured experimental propagation speed over stretch rate. Three distinct flame regimes can be identified: (1) the ignition-energy-induced flame kernel propagation regime, (2) the normal flame propagation regime, and

(3) the radiation-induced regime. These three regimes are described in the following and can be clearly observed in Fig. 5 for the conditions at $P_0 = 5$ bar & $\phi = 1.06$, and $P_0 = 3$ bar & $\phi = 1.23$. In the first regime, the flame kernel propagation is mainly driven by ignition energy deposition. Both flame propagation and stretch decrease as the ignition kernel propagates outwardly until it reaches a critical radius, which is in those cases at $R_f = 0.9$ cm. Note that a successful ignition is only achieved when the ignition kernel can propagate beyond the critical flame initiation radius. Subsequently, the flame propagation speed is only affected by stretch rate, which represents the second regime. One can see that $S_{L,b}$ changes almost linearly with K. Hence, this regime is used to deduce the unstretched laminar flame speed and the burned-gas Markstein length $\mathcal{L}_b$, which represents the sensitivity of flame speed to stretch.

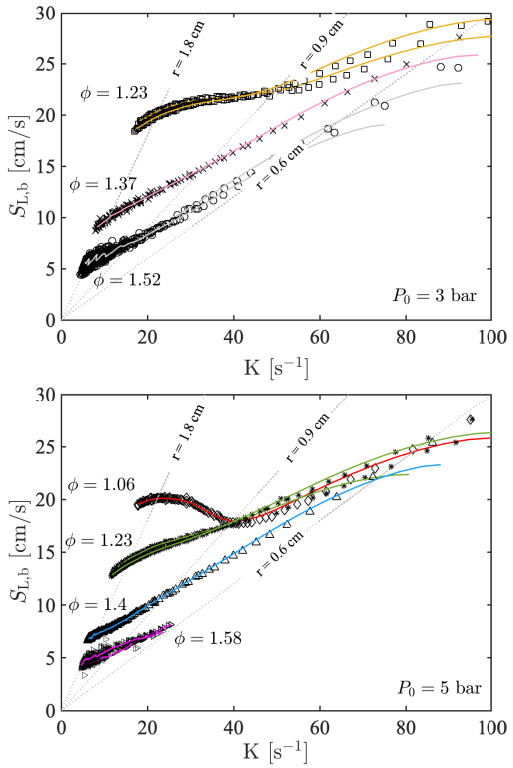

Fig. 5: Evolution of the propagation speed as a function of the flame stretch for ethanol mixtures at two initial pressures of 3 and 5 bar, and various equivalence ratios shown by different symbols. Lines represent the filtered data.

In the third regime and for small stretch rates, $S_{L,b}$ does not linearly evolve with K, but rather reaches a maximum and then decreases. There are two major reasons for this decrease: the first one is the slight pressure increase in the spherical chamber because the valves open once 0.025 MPa increase is reached, and the second is radiation effects. Chen [23] performed detailed numerical simulations of radiation in spherical flames and demonstrated that radiation heat loss decreases the flame speed via two mechanisms: (1) a thermal-flow effect caused by the burned gas cooling, which generates an inward flow towards the cooling core of the burned gas region and a reduction of the flame's expansion velocity, and (2) a thermal-chemical effect caused by the decreased flame temperature, which slows the actual flame propagation because of a decrease in the overall reaction rate. Three ways to correct for radiation heat losses can be found in the literature. The first one is to perform DNS together with employing a statistical narrow band model (SNB). The SNB considers reabsorption by unburned gas and therefore gives quite accurate predictions. However, combining a DNS with an SNB model is computationally expensive, especially when the reaction mechanism used contains a large amount of species and reactions. The second way is to use an empirical formula proposed by Yu et al. [14], which was developed by employing DNS and the SNB model and considers corrections both of the thermal-flow and the thermal-chemical effects (cf. Eq. (2) in Section 4.2.2). The third method is to apply the analytical model by Santner et al. [13], which estimates the thermal and flow effects caused by radiation separately.

In our recent work [12], we employed the Santner et al. [13] model. We showed that without using the radiation correction for refrigerant flames, the obtained flame speeds would be 15% to 20% lower than using the correction. However, the Santner et al. [13] analytical model is not applicable in the present work because it does not capture the high N_2-dilution levels involved in the mixtures investigated. This can be seen in Fig. S3 of the Supplementary Material, where the temperature decay due to radiation heat losses is found to be marginal.

For the larger equivalence ratios shown in Fig 5, the propagation speed $S_{L,b}$ decreases with the decreasing stretch rate K as the flame propagates outwardly resulting in negative burned-gas Markstein length, $\mathcal{L}_b$. The effect of stretch on the flame speed changes with equivalence ratio. Moreover, the change of $S_{L,b}$ with the stretch rate is reasonably linear over the measured range of flame radius. It is worth noting that the decay in $S_{L,b}$ observed previously vanishes when ϕ becomes even richer. Consequently, a linear extrapolation of $S_{L,b}$ to zero stretch can be applied to obtain the unstretched propagation speed. A similar behavior was obtained by Wang et al. [24] investigating the flammability limits of methane flames under microgravity conditions.

The effect of pressure is also investigated at a fixed equivalence ratio $\phi = 1.23$ and the results are shown in Fig. 6. As expected, the propagation speed decreases with increasing pressure. Negative burned-gas Markstein lengths are obtained with higher magnitude for higher pressures.

4.2.2. Laminar flame speed

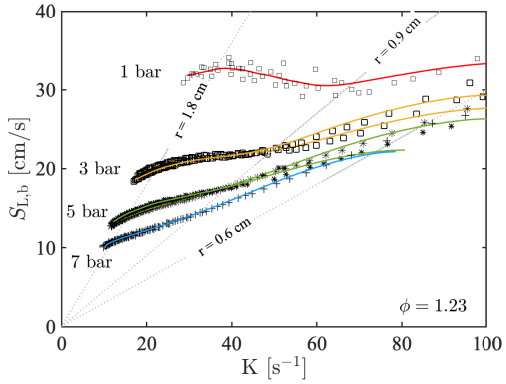

Fig. 6: Evolution of the propagation speed as a function of the flame stretch for ethanol-rich mixtures at different initial pressures shown by different symbols. Lines represent the filtered data.

The flame-radii range to be used to extrapolate back to zero-stretch is of paramount importance and should be carefully selected. The lower limit is usually chosen to reduce the effects of initial spark ignition, and the upper bound is often selected to ensure that the pressure change does not exceed 1%. Several extrapolation techniques exist, for instance, the linear [25] and non-linear methods [26, 27]. Assessments of these techniques have been presented in the literature [28, 29].

Due to the non-linearity of radiation for cases at $P_0 = 5$ bar & $\phi = 1.06$ and $P_0 = 3$ bar & $\phi = 1.23$, extrapolation can involve large errors. For this reason, the flame radius-range used for those specific conditions was limited to flames where no decay in the flame propagation speed $S_{\mathrm{L,b}}$ was observed, which is linked to a nonzero burned gas velocity resulting in slowing down the flame propagation. This means that the radius range considered is 0.9 cm $\leq R_{\mathrm{f}} \leq$ 1.5 cm. For the remaining conditions, the extrapolation was straightforward, and a linear method is applied for a radius ranging between 0.9 cm $\leq R_{\mathrm{f}} \leq$ 1.8 cm.

After extrapolating back to zero-stretch, i.e., $S^0_{\mathrm{L,b}}$, the laminar flame speed is determined from mass continuity through a planar unstretched flame, $S^0_{\mathrm{L,u}} = \rho_{\mathrm{b}}/\rho_{\mathrm{u}}\, S^0_{\mathrm{L,b}}$, where ρ_{b} and ρ_{u} represent the burned- and unburned-gas densities. It is important to highlight that these results are radiation-affected and are shown in Fig. 7 over the equivalence ratio (filled symbols). The lines in Fig. 7 represent laminar flame speeds obtained from adiabatic unstretched premixed simulations using the kinetic mechanism by Cai et al. [22]. The total differences between radiation-induced flame speeds and simulations are in the order of 10% near stoichiometric conditions and become larger to approximately 45% at fuel-rich conditions. These results were expected since the experimental data obtained are not yet radiation corrected. The change in laminar flame speed is clearly non-negligible for the conditions investigated and would be even more pronounced for fuels with a high sooting tendency. A radiation-correction is therefore necessary.

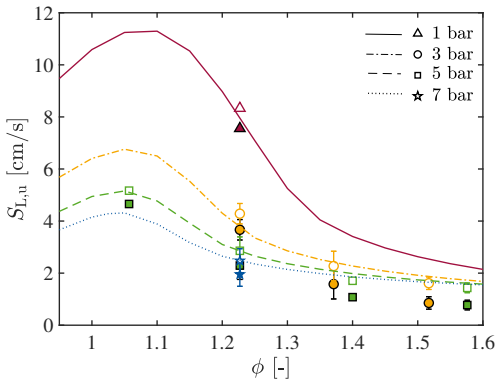

Fig. 7: Laminar flame speed vs equivalence ratio. Filled and open symbols correspond to non- and radiation corrected flame speeds, respectively. Lines represent results obtained using the mechanism by Cai et al. [22].

A radiation correction is conducted as a final step. The generalized empirical correlation by Yu et al. [14] is used to obtain radiation-free laminar flame speeds. Recall that this model was developed by employing DNS and the SNB model. It is also based on several types of fuels, from C_1 to C_8 hydrocarbon fuels, syngas H_2/CO at various ratios, and fuels containing oxygen functional groups such as dimethyl ether. This indicates that the model should be applicable for alcohols, such as ethanol. Moreover, a wide range of equivalence ratios and different initial pressures and temperatures were chosen to quantify the uncertainty associated with radiation. It is also important to highlight that the flame radius range, similar to our experiments, of 1.0 cm $\leq R_{\mathrm{f}} \leq$ 2.0 cm was selected to deduce their correlation. Thus, the correlation considers also the contraction velocity effect appropriately. It is given as

$$\frac{S^{\mathrm{corr}}_{\mathrm{L,u}}}{S_{\mathrm{L,u}}} = 1 + 0.82 \left(\frac{S_{\mathrm{L,u}}}{S_0}\right)^{-1.14} \left(\frac{T_0}{T_i}\right) \left(\frac{P}{P_i}\right)^{-0.3}, \quad (2)$$

where $S_0 = 1$ cm/s, $T_i = 298$ K, and $P_i = 1$ atm.

Radiation-corrected laminar flame speeds obtained using Eq. (2) are shown in Fig. 7 by open symbols. The corrected experimental results and the predicted data are now comparable and agree very well, especially on the rich side, where a wider flame-radius range was used. The choice of the radius range to extrapolate back to zero stretch can significantly affect the results when radiation due to flow effects is pronounced. Therefore, the obtained experimental data, which were extremely difficult to measure and post-processed very carefully, can be used as a reference data set to validate kinetic schemes.

It is worth stressing that, because the flame thickness cannot be extracted experimentally, it was evaluated using the 1D unstretched laminar flame configuration of the open-source FlameMaster code [21],

where the mechanism by Cai et al. [22] was employed. The flame thickness increases as the mixture becomes richer for a defined initial pressure. From dimensional analysis ($S_{\mathrm{L,u}} = \mathcal{D}/l_{\mathrm{f}}$, where $\mathcal{D}$ is the thermal diffusivity), the laminar flame speed is reciprocal to the flame thickness l_{f}. The time scales become longer. Thus, the relative radiation heat loss effect on the flame speed becomes significant.

5. Concluding remarks

An experimental study was carried out to investigate laminar flame speeds of premixed ethanol/O_2/N_2 mixtures with very high N_2-dilution. These flames exhibit very low burning velocities that are difficult to measure quantitatively with good accuracy. The severe flame-front distortion under terrestrial gravity is shown by conducting experiments using the high-pressure, high-temperature RWTH spherical chamber employing a Schlieren optical technique to visualize the flame front propagation. Part of the difficulty stems from the fact that the flames become more sensitive to experimental errors when they burn with low propagation speeds. The effect of buoyancy was suppressed under microgravity conditions in a series of parabolic flights onboard the Airbus A310 Zero-G. The setup used at reduced gravity consists of a pressure-release-type dual chamber adequate for aircraft-related safety requirements, combined with a conventional shadowgraphy system to visualize the flame morphology. Unstretched 1D freely propagating flame simulations were performed using the Cai et al. [22] mechanism and were compared to the experimental data, both non-radiation-corrected or radiation-corrected, with the model given by Yu et al. [14]. The main outcomes of the present study are summarized as follows:

- Under reduced gravity, the flame expands in a spherical manner until it reaches the windows' limit. The propagation speeds were deduced based on the flame radius detected from shadowgraph images. A pronounced decrease in the burned-gas propagation speed owing to the nonzero burned-gas velocity is observed at large flame radii.
- Flame speed reduction induced by radiation is found to be in the order of 10% to 45% for the near-stoichiometric to very rich conditions, respectively. Radiation-corrected laminar flame speeds were obtained by applying the empirical correlation presented by Yu et al. [14]. Excellent agreement between the corrected experimental results and the predicted ones using the Cai et al. [22] mechanism is observed, highlighting that the new provided data can be used as a reference to validate/improve kinetic schemes.

Acknowledgments

The authors gratefully acknowledge the financial support provided by the Deutsches Zentrum fur Luft- und Raumfahrt (DLR, German Aerospace Center), Grant no. 50WM2073. We are also thankful to the ICARE laboratory.

Supplementary material

Supplementary material associated with this article can be found, in the online version, at doi:

References

[1] L. Qiao, Y. Gu, W. Dahm, E. Oran, G. Faeth, A study of the effects of diluents on near-limit h2–air flames in microgravity at normal and reduced pressures, Combust. Flame 151 (1-2) (2007) 196–208.

[2] L. Qiao, Y. Gan, T. Nishiie, W. Dahm, E. Oran, Extinction of premixed methane/air flames in microgravity by diluents: Effects of radiation and lewis number, Combust. Flame 157 (8) (2010) 1446 – 1455.

[3] W. Zhang, Z. Chen, W. Kong, Effects of diluents on the ignition of premixed h2/air mixtures, Combust. Flame 159 (1) (2012) 151–160.

[4] C. Liao, N. Saito, Y. Saso, Y. Ogawa, Flammability limits of combustible gases and vapors measured by a tubular flame method, Fire Saf. J. 27 (1) (1996) 49–68.

[5] E. Hu, J. Fu, L. Pan, X. Jiang, Z. Huang, Y. Zhang, Experimental and numerical study on the effect of composition on laminar burning velocities of h2/co/n2/co2/air mixtures, Int. J. Hydrogen Energy 37 (23) (2012) 18509–18519.

[6] A. Holley, X. You, E. Dames, H. Wang, F. N. Egolfopoulos, Sensitivity of propagation and extinction of large hydrocarbon flames to fuel diffusion, Proc. Combust. Inst. 32 (1) (2009) 1157–1163.

[7] T. Poinsot, Prediction and control of combustion instabilities in real engines, Proc. Combust. Inst. 36 (1) (2017) 1–28.

[8] U. Pfahl, M. Ross, J. Shepherd, K. Pasamehmetoglu, C. Unal, Flammability limits, ignition energy, and flame speeds in H2–CH4–NH3–N2O–O2–N2 mixtures, Combust. Flame 123 (1) (2000) 140 – 158.

[9] Z.-Y. Sun, G.-X. Li, H.-M. Li, Y. Zhai, Z.-H. Zhou, Buoyant unstable behavior of initially spherical lean hydrogen-air premixed flames, Energies 7 (8) (2014) 4938–4956.

[10] L. Berger, R. Hesse, K. Kleinheinz, M. J. Hegetschweiler, A. Attili, J. Beeckmann, G. T. Linteris, H. Pitsch, A DNS study of the impact of gravity on spherically expanding laminar premixed flames, Combust. Flame 216 (2020) 412 – 425.

[11] M. J. Hegetschweiler, J. L. Pagliaro, L. Berger, R. Hesse, J. Beeckmann, C. Bariki, H. Pitsch, G. T. Linteris, Data Reduction Considerations for Spherical R-32(CH2F2)-Air Flame Experiments, Combust. Flame 237 (2022) 111806.

[12] R. Hesse, L. Berger, C. Bariki, M. J. Hegetschweiler, G. T. Linteris, H. Pitsch, J. Beeckmann, Low global-warming-potential refrigerant CH2F2 (R-32): Integration of a radiation heat loss correction method to accurately determine experimental flame speed metrics, Proc. Combust. Inst. 38 (3) (2021) 4665–4672.

[13] J. Santner, F. Haas, Y. Ju, F. Dryer, Uncertainties in interpretation of high pressure spherical flame propagation rates due to thermal radiation, Combust. Flame 161 (1) (2014) 147–153.

[14] H. Yu, W. Han, J. Santner, X. Gou, C. H. Sohn, Y. Ju, Z. Chen, Radiation-induced uncertainty in lam-

inar flame speed measured from propagating spherical flames, Combust. Flame 161 (11) (2014) 2815–2824.
[15] G. Renoux, F. Halter, C. Chauveau, Experimental study of the morphology of two-phase flame instabilities in microgravity, Atomizat. Sprays 28 (10) (2018) 915–929.
[16] R. Thimothée, C. Chauveau, F. Halter, I. Gökalp, Experimental investigation of the passage of fuel droplets through a spherical two-phase flame, Proc. Combust. Inst. 36 (2) (2017) 2549–2557.
[17] C. Bariki, R. Hesse, F. Halter, H. Pitsch, J. Beeckmann, Combined isochoric and isobaric acquisition methodology for accurate flame speed measurements from ambient to high pressures and temperatures, Proc. Combust. Inst. 38 (2) (2021) 2185–2193.
[18] J. Beeckmann, L. Cai, H. Pitsch, Experimental investigation of the laminar burning velocities of methanol, ethanol, n-propanol, and n-butanol at high pressure, Fuel 117, Part A (2014) 340–350.
[19] Y. Wu, S. Panigrahy, A. Sahu, C. Bariki, J. Beeckmann, J. Liang, A. Mohamed, S. Dong, C. Tang, H. Pitsch, Z. Huang, H. Curran, Understanding the antagonistic effect of methanol as a component in surrogate fuel models: A case study of methanol/n-heptane mixtures, Combust. Flame 226 (2021) 229–242.
[20] M. R. Brooks, D. A. Crowl, Flammability envelopes for methanol, ethanol, acetonitrile and toluene, . Loss Prev. Process. Ind. 20 (2) (2007) 144–150.
[21] H. Pitsch, Flamemaster: A C++ computer program for 0d combustion and 1d laminar flame calculations (1998).
[22] L. Cai, H. Minwegen, S. Kruse, R. Büttgen, R. Hesse, A. Ramalingam, J. Beeckmann, K. Leonhard, K. Heufer, H. Pitsch, Exploring the combustion chemistry of a novel lignocellulose-derived biofuel: cyclopentanol. part ii: experiment, model validation, and functional group analysis, Combust. Flame 210 (2019) 134–144.
[23] Z. Chen, Effects of radiation and compression on propagating spherical flames of methane/air mixtures near the lean flammability limit, Combust. Flame 157 (2010) 2267–2276.
[24] S. Wang, H. Zhang, J. Jarosinski, A. Gorczakowski, J. Podfilipski, Laminar burning velocities and markstein lengths of premixed methane/air flames near the lean flammability limit in microgravity, Combust. Flame 157 (4) (2010) 667–675.
[25] M. Matalon, B. J. Matkowsky, Flames as gas dynamic discontinuities, J. Fluid Mech. 124 (1982) 239–259.
[26] F. Halter, T. Tahtouh, C. Mounaim-Rousselle, Nonlinear effects of stretch on the flame front propagation, Combust. Flame 157 (10) (2010) 1825–1832.
[27] A. Kelley, J. Bechtold, C. Law, Premixed flame propagation in a confining vessel with weak pressure rise, J. Fluid Mech. 691 (2012) 26–51.
[28] F. Wu, W. Liang, Z. Chen, Y. Ju, C. K. Law, Uncertainty in stretch extrapolation of laminar flame speed from expanding spherical flames, Proc. Combust. Inst. 35 (1) (2015) 663–670.
[29] J. Beeckmann, R. Hesse, J. Schaback, H. Pitsch, E. Varea, N. Chaumeix, Flame propagation speed and markstein length of spherically expanding flames: Assessment of extrapolation and measurement techniques, Proc. Combust. Inst. 37 (2) (2019) 1521–1528.